LETTERS

Antioxidant and oncogene rescue of metabolic defects caused by loss of matrix attachment

Zachary T. Schafer[1]†, Alexandra R. Grassian[1]*, Loling Song[1]*, Zhenyang Jiang[1], Zachary Gerhart-Hines[2,3], Hanna Y. Irie[1], Sizhen Gao[1], Pere Puigserver[1,2] & Joan S. Brugge[1]

Normal epithelial cells require matrix attachment for survival, and the ability of tumour cells to survive outside their natural extracellular matrix (ECM) niches is dependent on acquisition of anchorage independence[1]. Although apoptosis is the most rapid mechanism for eliminating cells lacking appropriate ECM attachment[2], recent reports suggest that non-apoptotic death processes prevent survival when apoptosis is inhibited in matrix-deprived cells[3,4]. Here we demonstrate that detachment of mammary epithelial cells from ECM causes an ATP deficiency owing to the loss of glucose transport. Overexpression of ERBB2 rescues the ATP deficiency by restoring glucose uptake through stabilization of EGFR and phosphatidylinositol-3-OH kinase (PI(3)K) activation, and this rescue is dependent on glucose-stimulated flux through the antioxidant-generating pentose phosphate pathway. Notably, we found that the ATP deficiency could be rescued by antioxidant treatment without rescue of glucose uptake. This rescue was found to be dependent on stimulation of fatty acid oxidation, which is inhibited by detachment-induced reactive oxygen species (ROS). The significance of these findings was supported by evidence of an increase in ROS in matrix-deprived cells in the luminal space of mammary acini, and the discovery that antioxidants facilitate the survival of these cells and enhance anchorage-independent colony formation. These results show both the importance of matrix attachment in regulating metabolic activity and an unanticipated mechanism for cell survival in altered matrix environments by antioxidant restoration of ATP generation.

Epithelial cells are dependent on interactions with specific ECM components for survival, proliferation and differentiation functions[5]. Loss of matrix attachment of cultured epithelial cells activates a caspase-mediated apoptotic program known as anoikis[2]. In glandular cancers, such as breast cancer, tumour cells are displaced from their normal matrix niches in the early stages of tumorigenesis when they proliferate into the lumen of hollow glandular structures. Filling of the luminal space is one of the hallmarks of early tumorigenesis.

Studies of luminal filling in three-dimensional (3D) structures of MCF-10A mammary epithelial cells and the developing mammary gland have demonstrated that apoptosis is involved in the clearance of centrally localized cells that lack matrix attachment; however, inhibition of apoptosis is not sufficient for the survival of matrix-deprived cells in the luminal space[3,4,6,7]. Notably, several oncogenes, including ERBB2, have been shown to rescue cells from anoikis and prevent clearance of luminal cells in 3D acinar structures[8], suggesting that these oncogenes prevent luminal clearance programs in addition to anoikis.

Another distinct feature of both matrix-detached MCF-10A cells and centrally located, matrix-deprived cells in MCF-10A acini is the induction of autophagy[9,10]. Because autophagy is a catabolic process commonly upregulated under conditions of starvation[11], the association of this process with matrix deprivation suggests that ECM attachment regulates metabolic activity as well as apoptosis. Here we determine the basis for the metabolic defects in matrix-detached cells, demonstrate that oncogenes can rescue these defects by restoration of glucose uptake and enhancement of antioxidant capacity, and unexpectedly find that antioxidants alone can rescue matrix-detached cells by restoration of ATP generation through fatty acid oxidation (FAO). Furthermore, we demonstrate that antioxidants promote anchorage-independent survival in two *in vitro* models of tumorigenesis.

To investigate whether ECM regulates cellular metabolism, we examined cellular ATP levels in MCF-10A cells cultured on adherent or non-adherent plates. We detected a substantial reduction in ATP in both MCF-10A (Fig. 1a) and primary human mammary epithelial cells (HMEC; Supplementary Fig. 2) that had been detached from the ECM for 24 h. We confirmed these results in lysates normalized for total protein (Fig. 1b) and by measuring the ATP/ADP ratio (Fig. 1c). The reduction of ATP in MCF-10A cells occurred between 12 and 24 h after ECM detachment (Supplementary Fig. 7), was not affected by inhibition of apoptosis (Fig. 1a and Supplementary Figs 4 and 5) or autophagy (Supplementary Fig. 6), and was rescued by the addition of reconstituted basement membrane (Supplementary Fig. 3). The expression of ERBB2 in these cells (ERBB2-MCF-10A) prevented the reduction in ATP after matrix detachment (Fig. 1a, c), suggesting that ERBB2 circumvents the matrix requirement for ATP production.

Given the evidence that EGFR is downregulated in detached cells and that its overexpression can rescue anoikis[12], we investigated the effect of ERBB2 on EGFR expression in detached cells. Indeed, ERBB2 expression caused a marked stabilization of EGFR after ECM detachment (Fig. 1d) that was critical for the rescue of ATP (Fig. 1e). This stabilization correlated with the maintenance of ERK1 and ERK2 (also known as MAPK3 and MAPK1, respectively) activation and an enhancement of PI(3)K–AKT signalling (Fig. 1d); however, inhibition of PI(3)K (but not ERK) abrogated the ERBB2 rescue of ATP (Fig. 1f, g). Furthermore, expression of a constitutively active variant of PI(3)K (PIK3CA(E545K)) or AKT (Myr-AKT1) is sufficient to rescue detachment-induced ATP (Fig. 1h). These results indicate that ERBB2 rescues the metabolic defect in matrix-detached cells by preventing the downregulation of EGFR and thus maintaining the activation of the PI(3)K pathway.

Given the critical role of PI(3)K–AKT in stimulating glucose transport[13,14], we investigated whether glucose uptake is altered in matrix-detached cells. Indeed, we found a marked deficiency in glucose uptake in detached cells that was rescued (in a PI(3)K-dependent

[1]Department of Cell Biology, Harvard Medical School, Boston, Massachusetts 02115, USA. [2]Department of Cancer Biology, Dana-Farber Cancer Institute, Boston, Massachusetts 02115, USA. [3]Department of Cell Biology, Johns Hopkins University School of Medicine, Baltimore, Maryland 21205, USA. †Present address: Department of Biological Sciences, University of Notre Dame, Notre Dame, Indiana 46556, USA.
*These authors contributed equally to this work.

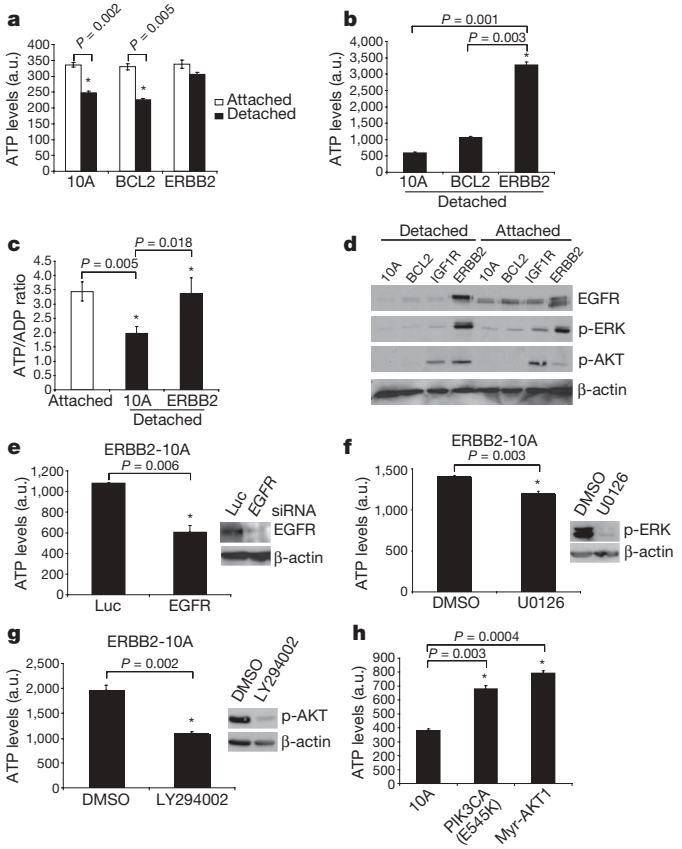

Figure 1 | Loss of matrix attachment causes reduction in cellular ATP that is rescued by ERBB2 through PI(3)K pathway activation. **a**, **b**, ATP was measured in the indicated cells 24 h after plating in adherent or non-adherent (poly-HEMA-coated) plates using the ATPlite assay (**a**) or the ATP determination kit (**b**). **c**, The ATP/ADP ratio was measured in the indicated cells. **d**, The indicated cells were immunoblotted for EGFR, phosphorylated (p)-ERK, p-AKT or β-actin. IGF1R cells were used as a positive control for p-AKT. **e**, ERBB2-MCF-10A cells were transfected with siRNAs targeting luciferase (luc) or *EGFR*, and ATP levels were measured using the ATP determination kit. Knockdown was confirmed by immunoblot. **f**, **g**, Detached ERBB2-MCF-10A cells were treated with 10 μM UO126 (ERK pathway inhibitor) (**f**) or 50 μM LY294002 (PI(3)K inhibitor) (**g**) for 24 h, and ATP was measured using the ATP determination kit. Inhibition was confirmed by immunoblotting. **h**, ATP was measured in detached 10A cells or 10A cells expressing PIK3CA(E545K) or Myr-AKT1 using the ATP determination kit. All error bars represent s.d. ($n = 3$). Asterisks denote statistically significant change calculated using a two-tailed *t*-test. a.u., arbitrary units.

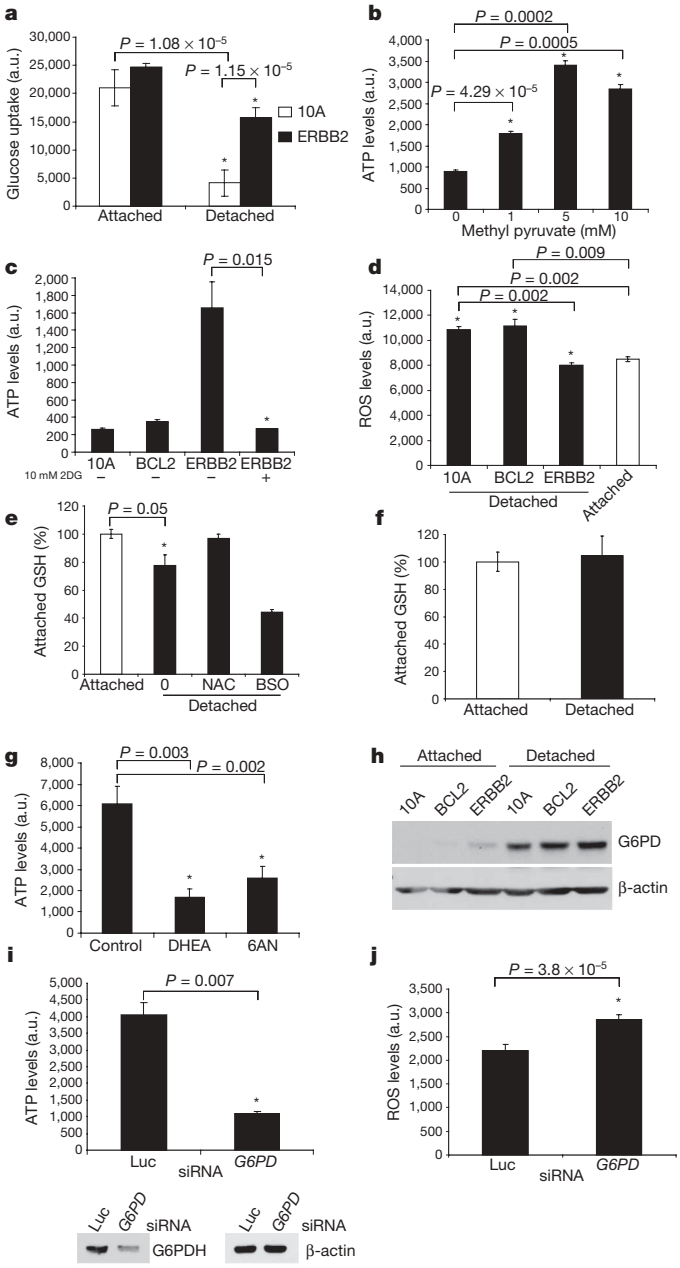

Figure 2 | Matrix detachment causes a reduction in glucose uptake and ERBB2 rescue of this defect is dependent on PPP flux. **a**, Glucose uptake was measured in the indicated cells using the Amplex Red assay. **b**, ATP was measured using the ATP determination kit after treatment (where indicated) of detached cells with methyl pyruvate. **c**, ATP was measured using the ATP determination kit after treatment (where indicated) of detached cells with 2DG. **d**, ROS was measured in attached and detached cells using DCF-DA. **e**, **f**, Reduced glutathione (GSH) was measured in 10A (**e**) or ERBB2-MCF-10A (**f**) cells. Results are shown as the percentage of the attached reduced GSH levels. NAC (1 mM) and BSO (1 mM; an inhibitor of glutathione synthesis) were used as a positive and negative control, respectively. **g**, ATP was measured using the ATP determination kit in detached ERBB2-MCF-10A cells after treatment (where indicated) with vehicle control, 150 μM DHEA, or 150 μM 6AN. **h**, The indicated cell lines were immunoblotted for G6PD after plating in either normal (attached) or poly-HEMA-coated (detached) plates. **i**, **j**, ATP (**i**) and ROS (**j**) were measured after siRNA-mediated knockdown of *G6PD* in detached ERBB2-MCF-10A cells. Knockdown was confirmed by immunoblotting. All error bars represent s.d. ($n = 3$). Asterisks denote statistical significance calculated using a two-tailed *t*-test.

fashion, Supplementary Fig. 8) by ERBB2 expression (Fig. 2a). Furthermore, treatment of detached cells with methyl pyruvate, which provides substrates for the tricarboxylic acid (TCA) cycle, causes a substantial increase in ATP (Fig. 2b) that is blocked by the mitochondrial complex 1 inhibitor rotenone (Supplementary Fig. 9). This suggests that the mitochondria of detached cells retain the capacity to produce ATP. To determine whether the rescue of glucose uptake by ERBB2 is important for its ability to increase ATP levels in detached cells, we treated ERBB2-MCF-10A cells with 2-deoxyglucose (2DG), a glucose analogue that inhibits glycolysis. 2DG treatment completely abolished the rescue of ATP by ERBB2 (Fig. 2c), confirming the importance of glucose uptake in the rescue of ATP by ERBB2.

After cellular uptake, glucose can be further metabolised to generate ATP by glycolysis/oxidative phosphorylation, or it can be driven down the pentose phosphate pathway (PPP) by glucose-6-phosphate dehydrogenase (G6PD)[15]. Because the PPP is an important source of cellular NADPH (which provides reducing equivalents), we examined the effects of matrix detachment on ROS production. ECM detachment induced a significant increase in ROS (Fig. 2d) and decrease in reduced glutathione (Fig. 2e), both of which were reversed by ERBB2 (Fig. 2d, f). In support of the possibility that the lack of PPP flux is responsible for the increase in ROS, we found that the reduction in

glucose uptake precedes the increase in ROS levels (Supplementary Fig. 10).

Previous studies have shown that reducing ROS through the stimulation of PPP flux can promote cell survival[16,17]; thus we proposed that PPP flux may be important for ERBB2 to rescue ATP levels in detached cells. Indeed, the treatment of detached ERBB2-MCF-10A cells with the PPP inhibitors dehydroisoandrosterone (DHEA) or 6-aminonicotinamide (6AN) abrogated the ability of ERBB2 to rescue ATP (Fig. 2g) and led to an increase in cellular ROS (Supplementary Fig. 11). Interestingly, we found that matrix-detachment caused a significant increase in G6PD protein (Fig. 2h), and short interfering RNA (siRNA)-mediated reduction of G6PD in detached ERBB2-MCF-10A cells caused a substantial decrease in ATP levels (Fig. 2i) and increase in ROS (Fig. 2j). The evidence that loss of matrix attachment causes an increase is ROS is consistent with studies in endothelial cells[18] and in the developing mammary gland[4].

The induction of ROS in suspended cells led us to investigate the effects of ROS neutralization on ATP in matrix-detached cells. Treatment of detached MCF-10A cells with the antioxidants *N*-acetyl-L-cysteine (NAC) or Trolox (a water-soluble vitamin E derivative) significantly increased ATP in detached cells (Fig. 3a), independent of any changes in glucose uptake (Fig. 3b). These data suggest that ROS inhibits ATP production through a metabolic pathway that could otherwise compensate for loss of glucose uptake.

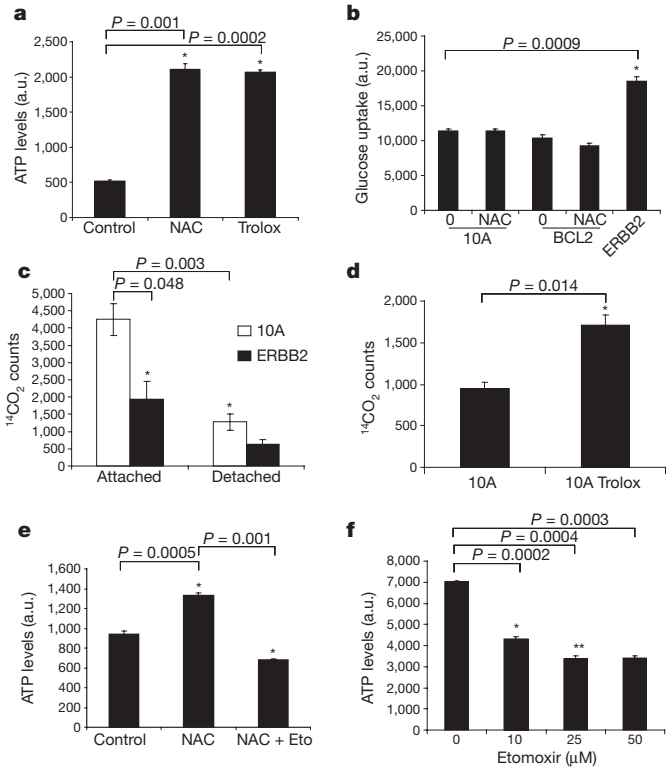

Figure 3 | Antioxidants rescue low ATP levels in detached cells by permitting fatty acid oxidation. **a**, MCF-10A cells were plated in poly-HEMA-coated plates and treated with control, 1 mM NAC or 50 μM Trolox, and ATP was measured using the ATP determination kit. **b**, Detached 10A or BCL2-MCF-10A cells were treated with either vehicle (0) or 1 mM NAC and glucose uptake was compared to ERBB2-MCF-10A cells using the Amplex Red assay. **c**, FAO was measured in parental or ERBB2-MCF-10A cells (either attached or detached). **d**, Detached MCF-10A cells were treated with either vehicle (10A) or 50 μM Trolox, and FAO was measured. **e**, Detached MCF-10A cells were treated with DMSO, 1 mM NAC, and/or 25 μM etomoxir (Eto) and ATP was measured using the ATP determination kit. **f**, Detached ERBB2-MCF-10A cells were treated with the indicated doses of etomoxir, and ATP was measured using the ATP determination kit. All error bars represent s.d. ($n = 3$). Asterisks denote statistical significance calculated using a two-tailed *t*-test.

It has previously been demonstrated that cancer cells deprived of glucose maintain ATP production through FAO[19]. Given that detached cells are glucose-deprived and antioxidants can promote ATP generation, we hypothesized that detachment-induced ROS could inhibit FAO. Indeed, we found that FAO was markedly reduced in detached MCF-10A cells (Fig. 3c) and Trolox treatment substantially increased FAO (Fig. 3d). In addition, treatment of antioxidant-supplemented cells with etomoxir, an inhibitor of fatty acid transport into the mitochondria[19], prevented the rescue of ATP by antioxidants in detached cells (Fig. 3e). Furthermore, methyl malate treatment (which generates NADPH through an alternative pathway) increased ATP levels, lowered ROS levels, and caused an increase in FAO in detached MCF-10A cells (Supplementary Fig. 12a–c) suggesting that NADPH production is sufficient to increase FAO. Notably, ERBB2 reduced FAO in attached and suspended cells (Fig. 3c), consistent with previous reports showing PI(3)K–AKT-mediated reduction of FAO[19,20]. However, treatment of detached ERBB2-MCF-10A cells with etomoxir caused a dose-dependent reduction in ATP levels (Fig. 3f), suggesting that the residual FAO significantly contributes to ATP production in these cells.

To extend our analysis to a model with more physiological relevance, we used the MCF-10A 3D cell culture model in which the inner, matrix-deprived cells show evidence of metabolic impairment (on the basis of upregulation of autophagy[9,10]). Although it is not feasible to measure ATP directly in these structures, we used two-photon microscopy to examine the native fluorescence of NADH and NADPH (NAD(P)H) and obtain an assessment of metabolic differences between the inner and outer cells[21]. Because NADH is the principal electron donor in glycolytic and oxidative metabolism, the native fluorescence of NAD(P)H represents a non-invasive fluorescent reporter of the metabolic state[22]. Images of acinar structures on day 8 showed a dichotomy in NAD(P)H fluorescence intensity between the inner and outer cells of most structures, whereas most day 4 structures showed homogenous fluorescence (Fig. 4a and Supplementary Fig. 13). Furthermore, we found that ROS were detectable exclusively in the centrally localized cells of day 7 acini (Fig. 4c). Together, there results provide evidence that there are differences in metabolic activity and ROS accumulation in the matrix-deprived centrally localized cells of acini, as were observed in monolayer and suspension cultures (Figs 1–3). In addition, Trolox treatment prevented the dichotomy in NAD(P)H fluorescence in 3D culture (Fig. 4b and Supplementary Fig. 14), suggesting that ROS significantly contributes to the metabolic dichotomy between the inner and outer cells.

To understand the implications of these findings with regards to the clearance of cells from the luminal space, we studied the effects of antioxidant treatment on the survival of cells located in the centre of acini. We treated acini with either NAC or Trolox and monitored luminal filling over time. Notably, we found that NAC or Trolox treatment significantly reduced luminal clearance (Fig. 4d) independent of effects on caspase activation (Supplementary Fig. 15), suggesting that the elimination of ROS can preserve the viability of matrix-deprived cells in the centre of acini. By extrapolation to our studies showing ATP reduction and ROS generation in matrix-deprived cells, we speculate that the viability is a consequence of rescuing these metabolic impairments. Furthermore, the late clearing of acini observed in BCL2-MCF-10A cells is suppressed by Trolox (Fig. 4d). These results indicate that suppression of both metabolic impairments and apoptosis are required for anchorage-independent survival.

The evidence that antioxidants can rescue metabolic defects of ECM-deprived cells and promote luminal filling in MCF-10A acini raises the question of whether antioxidants could promote the transforming activity of mammary epithelial cells. To examine this, we assayed anchorage-independent colony formation in soft agar in MCF-10A cells expressing oncogenes that promote hyperproliferation (human papilloma virus E7 protein) and suppress apoptosis (BCL2). Neither E7 nor BCL2 expression rescued ATP in matrix detached cells

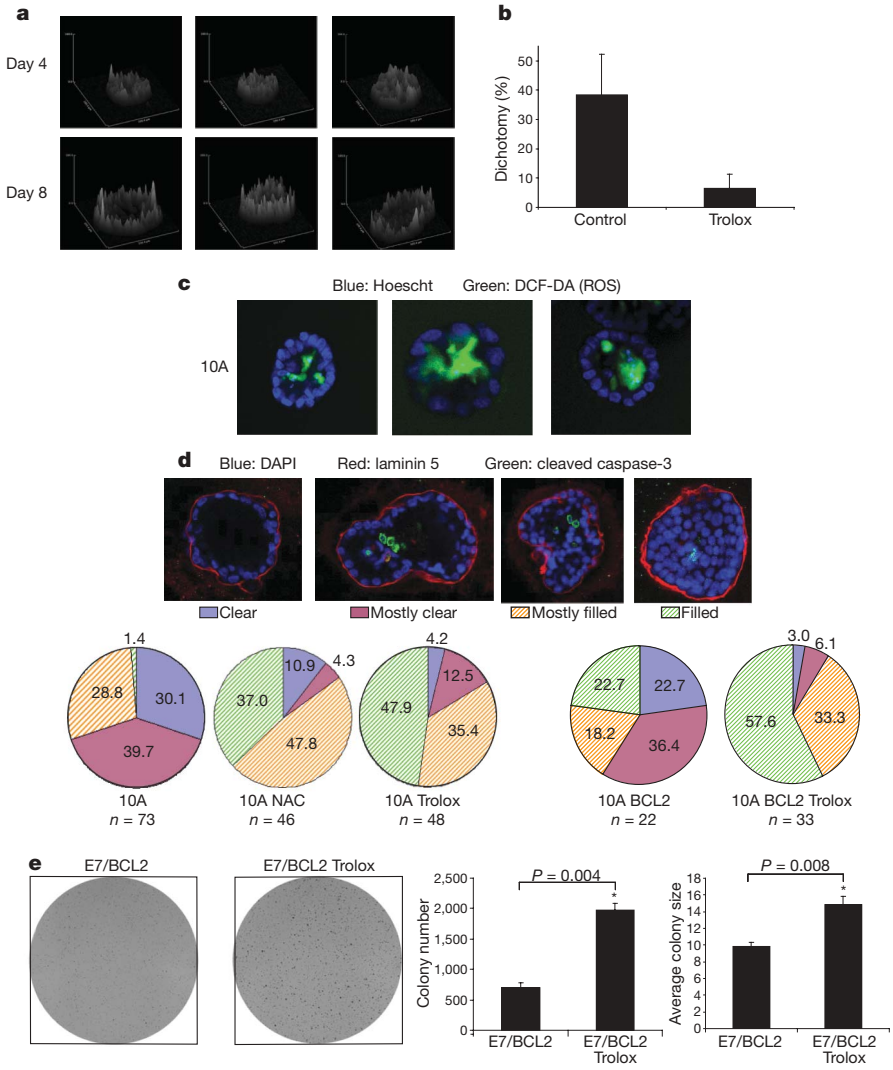

Figure 4 | Analysis of antioxidant effects on acinar morphogenesis and colony formation in soft agar. **a**, Native fluorescence of NAD(P)H was assayed by two-photon microscopy in MCF-10A acini. Surface intensity plots of three representative structures from day 4 or 8 are shown. **b**, Native fluorescence of NAD(P)H was assayed by two-photon microscopy in MCF-10A acini cultured in the presence or absence of 50 μM Trolox (added daily). At day 8, structures were blindly scored for dichotomy in fluorescent intensity on the basis of evidence of a reduction in fluorescence intensity in the inner cells (see examples in Supplementary Fig. 14). Error bars represent s.d. of individual scorings ($n = 5$). **c**, ROS was measured in MCF-10A acini at day 7, by staining with 25 μM DCF-DA (green) and Hoescht (blue). Three representative images are shown and 41% ($n = 73$) of all structures were positive for DCF-DA staining exclusively in the inner cells. NAC or Trolox treatment inhibited the DCF-DA staining in acini (data not shown). Original magnification, ×40. **d**, Acini were formed using 10A or BCL2-MCF-10A cells (10A or 10A BCL2) and treated with 1 mM NAC or 50 μM Trolox as indicated. At day 19 (10A) or day 33 (BCL2) acini were stained for laminin 5, cleaved caspase-3, and with the nuclear stain 4,6-diamidino-2-phenylindole (DAPI). Acini were then scored as described. Original magnification, ×40. **e**, 10A cells expressing E7 and BCL2 were plated in soft agar and after 20 days, images were taken after iodonitrotetrazolium chloride (also known as INT-violet) staining. Colony number and average colony size were determined using ImageJ. Error bars represent s.d. ($n = 3$ unless otherwise indicated). Asterisks represent statistical significance calculated using a two-tailed *t*-test.

(data not shown) and the E7/BCL2 cells exhibited a relatively weak capacity to form colonies in this assay (Fig. 4e). Trolox treatment induced a substantial increase in the number and average size of colonies, suggesting that antioxidant treatment can enhance the transforming activity of cells that contain oncogenic insults. We observed similar results with ERBB2-MCF-10A cells (Supplementary Fig. 16) and with BT-474 cells—an ERBB2-expressing breast cancer cell line (Supplementary Fig. 17).

Our study highlights the possibility that glucose deprivation could lead to ROS production during tumorigenesis and force selection for alterations that allow escape from oxidative damage. Furthermore, we demonstrate that antioxidants rescue cells from the need for glycolysis through stimulation of FAO. It has been shown previously that stimulation of FAO through AMP-activated protein kinase (AMPK) or p53 (also known as TP53) is another mechanism for the survival of cells in the absence of glucose[19]. Thus, our study suggests that deprivation of matrix may limit glucose accessibility during tumorigenesis, and reveals strategies in which a tumour could escape from metabolic stress owing to these conditions by stimulating anchorage-independent glucose transport and/or eliminating ROS.

These data also demonstrate that antioxidants promote the survival of cells that lack attachment to the ECM and raise the possibility that antioxidants may have dichotomous activities with respect to tumorigenesis—that is, suppressing tumorigenesis by preventing oxidative damage to DNA[23,24], and promoting tumorigenesis by allowing survival of cells that are metabolically impaired (for example, in altered matrix environments). In support of this, expression of SOD2, a mitochondrial protein that reduces oxidative stress caused by respiratory chain leak, is increased in more advanced and higher grade mammary tumours[25,26]. Furthermore, a recent study has revealed that enhanced PPP flux and increased antioxidant

capacity correlates with metastasis of breast cancer cells to the brain[27]. Lastly, randomized trials have demonstrated both anti-neoplastic and neoplastic effects of antioxidants, with neoplastic effects associated with patients at higher risk owing to smoking and alcohol consumption[28], or patients undergoing chemo- or radiation therapy[29]. Our work provides a biological rationale for these findings, as antioxidant activity may promote the survival of pre-initiated tumour cells in unnatural matrix environments and thus enhance malignancy.

METHODS SUMMARY

MCF-10A cells and their variants were all cultured as described at http://brugge.med.harvard.edu/. Other cell lines were cultured as described in the Supplementary Information. All assays on ECM-detached cells were carried out 24 h after plating on poly(2-hydroxyethyl methacrylate) (poly-HEMA)-coated plates unless otherwise noted. ATP assays were conducted using the ATPlite assay (PerkinElmer), the ATP determination kit (Invitrogen), or the ATP/ADP Ratio Assay Kit (BioAssay Systems). Glucose uptake assays were performed using the Amplex Red Glucose Assay Kit (Invitrogen). ROS was measured using carboxy-H_2DCF-DA in detached/attached cells and in 3D culture. To measure reduced glutathione, we used chloromethylcoumarin (CMAC, Invitrogen). FAO was measured by monitoring the release of $^{14}CO_2$ after the addition of 1-^{14}C-oleic acid. The 3D culture of mammary acini was completed according to the protocol at http://brugge.med.harvard.edu/. Native fluorescence of NADPH was measured using two-photon microscopy. Soft agar assays were performed in the presence or absence of antioxidants and colony formation/size was determined using ImageJ.

Full Methods and any associated references are available in the online version of the paper at www.nature.com/nature.

Received 13 March; accepted 6 July 2009.
Published online 19 August 2009.

1. Simpson, C. D., Anyiwe, K. & Schimmer, A. D. Anoikis resistance and tumor metastasis. *Cancer Lett.* **272,** 177–185 (2008).
2. Frisch, S. M. & Screaton, R. A. Anoikis mechanisms. *Curr. Opin. Cell Biol.* **13,** 555–562 (2001).
3. Debnath, J. *et al.* The role of apoptosis in creating and maintaining luminal space within normal and oncogene-expressing mammary acini. *Cell* **111,** 29–40 (2002).
4. Mailleux, A. A. *et al.* BIM regulates apoptosis during mammary ductal morphogenesis, and its absence reveals alternative cell death mechanisms. *Dev. Cell* **12,** 221–234 (2007).
5. Nelson, C. M. & Bissell, M. J. Of extracellular matrix, scaffolds, and signaling: tissue architecture regulates development, homeostasis, and cancer. *Annu. Rev. Cell Dev. Biol.* **22,** 287–309 (2006).
6. Debnath, J. & Brugge, J. S. Modelling glandular epithelial cancers in three-dimensional cultures. *Nature Rev. Cancer* **5,** 675–688 (2005).
7. Humphreys, R. C. *et al.* Apoptosis in the terminal endbud of the murine mammary gland: a mechanism of ductal morphogenesis. *Development* **122,** 4013–4022 (1996).
8. Muthuswamy, S. K. *et al.* ErbB2, but not ErbB1, reinitiates proliferation and induces luminal repopulation in epithelial acini. *Nature Cell Biol.* **3,** 785–792 (2001).
9. Fung, C. *et al.* Induction of autophagy during extracellular matrix detachment promotes cell survival. *Mol. Biol. Cell* **19,** 797–806 (2008).
10. Mills, K. R. *et al.* Tumor necrosis factor-related apoptosis-inducing ligand (TRAIL) is required for induction of autophagy during lumen formation *in vitro*. *Proc. Natl Acad. Sci. USA* **101,** 3438–3443 (2004).
11. Mathew, R., Karantza-Wadsworth, V. & White, E. Role of autophagy in cancer. *Nature Rev. Cancer* **7,** 961–967 (2007).
12. Reginato, M. J. *et al.* Integrins and EGFR coordinately regulate the pro-apoptotic protein Bim to prevent anoikis. *Nature Cell Biol.* **5,** 733–740 (2003).
13. Czech, M. P. & Corvera, S. Signaling mechanisms that regulate glucose transport. *J. Biol. Chem.* **274,** 1865–1868 (1999).
14. Elstrom, R. L. *et al.* Akt stimulates aerobic glycolysis in cancer cells. *Cancer Res.* **64,** 3892–3899 (2004).
15. DeBerardinis, R. J., Lum, J. J., Hatzivassiliou, G. & Thompson, C. B. The biology of cancer: metabolic reprogramming fuels cell growth and proliferation. *Cell Metab.* **7,** 11–20 (2008).
16. Bensaad, K. *et al.* TIGAR, a p53-inducible regulator of glycolysis and apoptosis. *Cell* **126,** 107–120 (2006).
17. Boada, J. *et al.* Cells overexpressing fructose-2,6-bisphosphatase showed enhanced pentose phosphate pathway flux and resistance to oxidative stress. *FEBS Lett.* **480,** 261–264 (2000).
18. Li, A. E. *et al.* A role for reactive oxygen species in endothelial cell anoikis. *Circ. Res.* **85,** 304–310 (1999).
19. Buzzai, M. *et al.* The glucose dependence of Akt-transformed cells can be reversed by pharmacologic activation of fatty acid β-oxidation. *Oncogene* **24,** 4165–4173 (2005).
20. Deberardinis, R. J., Lum, J. J. & Thompson, C. B. Phosphatidylinositol 3-kinase-dependent modulation of carnitine palmitoyltransferase 1A expression regulates lipid metabolism during hematopoietic cell growth. *J. Biol. Chem.* **281,** 37372–37380 (2006).
21. Bennett, B. D. *et al.* Quantitative subcellular imaging of glucose metabolism within intact pancreatic islets. *J. Biol. Chem.* **271,** 3647–3651 (1996).
22. Chance, B., Cohen, P., Jobsis, F. & Schoener, B. Intracellular oxidation-reduction states *in vivo*. *Science* **137,** 499–508 (1962).
23. Gao, P. *et al.* HIF-dependent antitumorigenic effect of antioxidants *in vivo*. *Cancer Cell* **12,** 230–238 (2007).
24. Narayanan, B. A. Chemopreventive agents alters global gene expression pattern: predicting their mode of action and targets. *Curr. Cancer Drug Targets* **6,** 711–727 (2006).
25. Ivshina, A. V. *et al.* Genetic reclassification of histologic grade delineates new clinical subtypes of breast cancer. *Cancer Res.* **66,** 10292–10301 (2006).
26. Sorlie, T. *et al.* Gene expression patterns of breast carcinomas distinguish tumor subclasses with clinical implications. *Proc. Natl Acad. Sci. USA* **98,** 10869–10874 (2001).
27. Chen, E. I. *et al.* Adaptation of energy metabolism in breast cancer brain metastases. *Cancer Res.* **67,** 1472–1486 (2007).
28. Omenn, G. S. *et al.* Effects of a combination of β carotene and vitamin A on lung cancer and cardiovascular disease. *N. Engl. J. Med.* **334,** 1150–1155 (1996).
29. Lawenda, B. D. *et al.* Should supplemental antioxidant administration be avoided during chemotherapy and radiation therapy? *J. Natl Cancer Inst.* **100,** 773–783 (2008).

Supplementary Information is linked to the online version of the paper at www.nature.com/nature.

Acknowledgements We thank M. Overholtzer, G. Mouneimne, M. Mazzone and C. Leung for critical reading of the manuscript and/or experimental assistance. We thank A. Mailleux, A. Kaanta, V. Schafer, A. Zhou, K. Simpson, and the members of the Brugge laboratory for experimental assistance, comments, and/or discussion. This work was supported by a grant from the National Cancer Institute (J.S.B.) and a grant from the National Institutes of Health (NIH) (P.P.). Z.T.S. is the recipient of a Ruth L. Kirschstein National Research Service Award (NRSA) for Postdoctoral Fellows from the National Cancer Institute; L.S. an NCI Mentored Quantitative Research Development Award (K25); A.R.G. a National Science Graduate Research Fellowship; and H.Y.I. an NCI K08 Award.

Author Contributions Z.T.S. and J.S.B. were responsible for the overall study design. Z.T.S., A.R.G., H.Y.I. and S.G. conducted experiments. L.S. and Z.J. conducted the experiments measuring native fluorescence of NADPH in 3D cell culture. Z.G.-H. and P.P. designed the fatty acid oxidation studies and Z.T.S. and Z.G.-H. conducted the fatty acid oxidation assays. Z.T.S. and J.S.B. drafted the manuscript and all other authors made revisions.

Author Information Reprints and permissions information is available at www.nature.com/reprints. Correspondence and requests for materials should be addressed to J.S.B. (joan_brugge@hms.harvard.edu).

METHODS

Cell culture. MCF-10A cells were cultured as described previously[30] and at http://brugge.med.harvard.edu/. MCF-10A cells expressing BCL2, ERBB2, E7/BCL2, PIK3CA(E545K), Myr-AKT1, IGF1R or GFP-LC3 were generated as described previously[3]. The pMSCV-Neo-based retroviral vectors encoding wild-type human *IGFIR* complementary DNA was a gift from R. Baserga. HMEC cells were immortalised with human TERT and cultured as described previously[31]. BT-474 cells (ATCC) were cultured in RPMI 1640 media plus 10% FBS and penicillin/streptomycin.

ATP assays. For the comparison of ATP levels in detached versus attached cells, the ATPlite assay (PerkinElmer) was used. Cells were plated in 96-well poly-HEMA-coated (or uncoated) plates at a density of 13,333 cells per well. After 24 h, ATP assay was conducted according to the manufacturer's protocol. For the measure of ATP in detached cells (normalized by protein content), the ATP determination kit (Invitrogen) was used. Cells were plated in 6-well poly-HEMA-coated plates at a density of 400,000 cells per well. After 24 h, cells were lysed in 1% NP40 (plus protease inhibitors) and lysates were normalized by protein content using BCA Protein Assay (Pierce Biotechnology). Lysates were then tested for ATP levels according to manufacturer's protocol. The data from these assays show representative experiments from more than three independent replicates. For determination of the ATP/ADP ratio, the ADP/ATP Ratio Assay Kit (BioAssay Systems) was used according to manufacturer's instructions. The data from the ATP/ADP assay is presented as an average of the ATP/ADP ratio from several experiments.

3D cell culture. To generate acini, cells were grown in reconstituted basement membrane (Matrigel) as described previously[30] and according to the protocol at http://brugge.med.harvard.edu/. For antioxidant treatment, either NAC or Trolox was added to the Matrigel and to the overlay media. Immunofluorescence of acini was performed as described previously[30]. The following primary antibodies were used for immunofluorescence: cleaved caspase-3 (Cell Signaling Technology) and laminin-5 (Millipore). DAPI (Sigma-Aldrich) was used to counterstain nuclei. For examination of luminal filling, acini were imaged using confocal microscopy to visualize the centre of each structure, and then were scored as clear (~90–100% clear), mostly clear (~50–90% clear), mostly filled (~10–50% clear), or clear (~0–10% clear). The figures including data from these assays show representative experiments from more than three independent replicates.

Reagents. The following reagents were used at the doses indicated and as described in the text/figure legends: methyl pyruvate (Sigma-Aldrich), 2-deoxy-D-glucose (Sigma-Aldrich), DHEA (EMD Biosciences), 6AN (Sigma-Aldrich), *N*-acetyl-L-cysteine (Sigma-Aldrich), Trolox (EMD Biosciences), etomoxir (Sigma-Aldrich), D-methyl malate (Sigma-Aldrich), Matrigel (BD Biosciences), poly(2-hydroxyethyl methacrylate) (poly-HEMA, Sigma-Aldrich), LY294002 (EMD Biosciences), U0126 (EMD Biosciences), staurosporine (Sigma-Aldrich), and DL-buthionine-(*S*,*R*)-sulphoximine (BSO, Sigma-Aldrich).

siRNA. The following siRNA SMARTpools (Dharmacon) were used: G6PD (M-008181-01), Beclin-1 (M-010552-00), ATG5 (M-004374-03), and EGFR (M-003114-01). The luciferase GL2 duplex (D-00110-01-20) was used as an siRNA control. Sequence information for each siRNA are as follows: G6PD SMARTpool, duplex 1, sense: GAGAGUGGGUUUCCAGUAUUU, antisense: 5′-PAUACUGGAAACCCACUCUCUU; duplex 2, sense: CAACAUCGCCUGCGUUAUCUU, antisense: 5′-PGAUAACGCAGGCGAUGUUGUU; duplex 3, sense: CGUGAGGCCUGGCGUAUUUUU, antisense: 5′-PAAAUACGCCAGGCCUCACGUU; duplex 4, sense: GACCUACGGCAACAGAUAUU, antisense: 5′-PUAUCUGUUGCCGUAGGUCAUU. Beclin-1 SMARTpool, duplex 1, sense: CUAAGGAGCUGCCGUUAUAUU, antisense: 5′-PUAUAACGGCAGCUCCUUAGUU; duplex 2, sense: GGAUGACAGUGAACAGUUAUU, antisense: 5′-PUAACUGUUCACUGUCAUCCUU; duplex 3, sense: UAAGAUGGGUCUGAAAUUUUU, antisense: 5′-PAAAUUUCAGACCCAUCUUAUU; duplex 4, sense: GCCAACAGCUUCACUCUGAUU, antisense: 5′-PUCAGAGUGAAGCUGUUGGCUU. ATG5 SMARTpool, duplex 1, sense: GGAAUAUCCUGCAGAAGAAUU, antisense: 5′-PUUCUUCUGCAGGAUAUUCCUU; duplex 2, sense: CAUCUGAGCUACCCGGAUAUU, antisense: 5′-PUAUCCGGGUAGCUCAGAUGUU; duplex 3, sense: GACAAGAAGACAUUAGUGAUU, antisense: 5′-PUCACUAAUGUCUUCUUGUCUU; duplex 4, sense: CAAUUGGUUUGCUAUUUGAUU, antisense: 5′-PUCAAAUAGCAAACCAAUUGUU. EGFR SMARTpool, duplex 1, sense: GAAGGAAACUGAAUUCAAAUU, antisense: 5′-PUUUGAAUUCAGUUUCCUUCUU; duplex 2, sense: GGAAAUAUGUACUACGAAAUU, antisense: 5′-PUUUCGUAGUACAUAUUUCCUU; duplex 3, sense: CCACAAAGCAGUGAAUUUAUU, antisense: 5′-PUAAAUUCACUGCUUUGUGGUU; duplex 4, sense: GUAACAAGCUCACGCAGUUUU, antisense: 5′-PAACUGCGUGAGCUUGUUACUU. Luciferase GL2 duplex, 5′-CGUACGCGGAAUACUUCGA dTdTdTdT GCAUGCGCCUUAUGAAGCU-5′.

For each transfection, 200 nM of siRNA was transfected into cells using oligofectamine (Invitrogen) according to manufacturer's protocol. Knockdown efficiency was examined after 48 h by western blotting as described later. For experiments involving siRNA in detached cells, cells were plated on poly-HEMA-coated plates 24 h after siRNA transfection and then assays were conducted 48 h after siRNA transfection. The figures including data using siRNAs show representative experiments from more than three independent replicates.

Western blotting. Cells were lysed in 1% NP40 on ice for 20 min. Lysates were spun at 16,000*g* at 4 °C for 30 min and normalized using a BCA Assay (Pierce Biotechnology). Lysates were then subjected to SDS–PAGE on polyacrylamide gels and transfer/blotting were performed as previously described[4]. The following antibodies were used for western blotting: G6PD (Abcam), Beclin-1 (Cell Signaling Technology), ATG5 (Cell Signaling Technology), cytochrome *c* (BD Biosciences), EGFR (Cell Signaling Technology), p-AKT (Cell Signaling Technology), p-ERK (Invitrogen) and β-actin (Sigma-Aldrich). The figures, including western blots, show representative blots from more than three independent experiments.

Cell death assays. Lysates preparation and the measurement of cytochrome *c* release were conducted as described previously[32]. For measuring viability by dye exclusion, detached or attached cells were stained with trypan blue and placed in a haemocytometer. Two-hundred cells were then counted and assessed as either trypan blue positive or negative.

Glucose uptake assay. For the analysis of glucose uptake, the Amplex Red Glucose Assay Kit (Invitrogen) was used. Cells were plated at a density of 13,333 cells per well in 96-well poly-HEMA-coated (or normal) plates. After 24 h, media was collected and diluted 1:4,000 in water. The amount of glucose in the media was then determined using the Amplex Red Assay according to the manufacturer's instructions. Glucose uptake was determined by subtracting the amount of glucose in each sample from the total amount of glucose in the media (without cells). The data from these assays show representative experiments from more than three independent replicates.

ROS and glutathione assays. Cells were plated at a density of 13,333 cells per well in 96-well poly-HEMA-coated (or normal) plates. After 24 h, carboxy-H_2DCFDA (Invitrogen) was added to each well at a concentration of 10 μM and mixed well. Carboxy-H_2DCFDA is a cell-permeant indicator for reactive oxygen species that is retained in the cell after deacetylation and non-fluorescent until oxidation occurs within the cell. After 2–3 h, absorbance was monitored using a fluorimeter. The figures including data from these assays show representative experiments from more than three independent replicates. Alternatively, reduced glutathione (GSH) was measured as a proxy for ROS using CMAC (Invitrogen)[33]. CMAC was added to detached or attached cells at 40 μM and fluorescence was measured at an excitation of 360 nm and an emission of 460 nm. For the measurement of ROS in MCF-10A acini, the acini were stained with 25 μM carboxy-H_2DCFDA and 1 μM Hoescht 33342 for 1 h at 37 °C. Acini were then immediately imaged using confocal microscopy.

FAO assay. Cells were plated at a density of 100,000 cells per well in 12-well poly-HEMA-coated (or normal) plates. After ~3–4 h, 100 μM oleic acid (Sigma-Aldrich) was added to each well. After 24 h, 1 μl of 1 μCi μl^{-1} [1-^{14}C]oleic acid (American Radiolabelled Chemicals) was added to each well and incubated at 37 °C for 1 h. To release $^{14}CO_2$, we then added 150 μl of 3 M perchloric acid (Fisher Scientific) to each well and immediately covered each well with phenylethylamine (Sigma-Aldrich)-saturated Whatman paper. Plate was then incubated at room temperature overnight and subsequently Whatman paper was removed, placed into Ready-Safe Liquid Scintillation Fluid (Beckman Coulter), and ^{14}C counts were read on scintillation counter. The figures including data from these assays show representative experiments from more than three independent replicates.

NAD(P)H fluorescence analyses. A two-photon excited fluorescence microscope was established on the basis of a Leica SP2 confocal microscope. It is equipped with a Ti:Sa laser (Spectral-Physics Broadband Mai Tai) with a tunable wavelength range of 710–990 nm, a pulse frequency of 80 MHz, and a pulse width (full-width at half-maximum (FWDM)) of 100 femtoseconds. The excitation wavelength was set to 730 nm. In the emission light path a SP700 short pass and BG39 filters were used to block any residual excitation photons. The fluorescence signal was filtered through a 505DCXR dichroic beam splitter (Chroma Technology) and wavelengths shorter than 505 nm were channelled to a Hamamatsu MCP-PMT detector. The effective spectral bandwidth of the detected fluorescence signal is 400–500 nm, corresponding to the maximum NADPH emission[34]. A ×63 (HCX PL APO 63X NA 1.2 W) water immersion objective lens was used for all the experiments. For each image, the emitted photons were collected for 5 min in the single photon counting mode (Becker & Hickl, SPC-830). All instrument settings and imaging parameters were maintained throughout the experiments. The images of photon counts are

displayed on the same intensity and spatial scales allowing for direct visual comparison.

MCF-10A cells were seeded on day 0 at a density of 5,000 cells per well in a coverslip-bottom 8-well chamber. On days 4 and 8, NAD(P)H fluorescence in 3D MCF-10A structures was imaged at the equatorial cross sections using two-photon fluorescence microscopy while being maintained on stage in a 37 °C chamber with 5% CO_2. For the antioxidant experiments (Fig. 4b) the two-photon excited native fluorescence images were acquired through non-descanned detection with a broadband emission filter (400–700 nm) and 730 nm excitation. Images were deconvolved by Huygens Professional (Scientific Volume Imaging). The images of more than 90 acinar structures were acquired on day 8 for either control or Trolox (50 μM) treatment. The randomized, blinded images were evaluated by five independent observers for the presence of NAD(P)H dichotomy (native fluorescence intensity difference between the inner and outer cells on the basis of images from the centre of each structure). For acini with filled lumen, an average from all five observers was derived from the positive scoring of a criterion. The standard deviation indicates the variation in a score among the five observers from this experiment.

Soft agar assays. Cells (4×10^4) were added to 1.5 ml (±antioxidants) of growth media plus 0.4% low-melt agarose (Sigma-Aldrich) and layered onto a 2-ml bed of growth media plus 0.5% low-melt agarose. Cells were fed every 2–3 days with 1 ml of growth media (±antioxidants). At the indicated times, growth media was removed and viable colonies were stained with iodonitrotetrazolium chloride (Sigma-Aldrich). Colony number and colony size were determined using ImageJ. The figures including data from these assays show representative experiments from more than three independent replicates.

30. Debnath, J., Muthuswamy, S. K. & Brugge, J. S. Morphogenesis and oncogenesis of MCF-10A mammary epithelial acini grown in three-dimensional basement membrane cultures. *Methods* **30,** 256–268 (2003).
31. Overholtzer, M. *et al.* Transforming properties of YAP, a candidate oncogene on the chromosome 11q22 amplicon. *Proc. Natl Acad. Sci. USA* **103,** 12405–12410 (2006).
32. Schafer, Z. T. *et al.* Enhanced sensitivity to cytochrome *c*-induced apoptosis mediated by PHAPI in breast cancer cells. *Cancer Res.* **66,** 2210–2218 (2006).
33. Sebastia, J. *et al.* Evaluation of fluorescent dyes for measuring intracellular glutathione content in primary cultures of human neurons and neuroblastoma SH-SY5Y. *Cytometry A* **51,** 16–25 (2003).
34. Vishwasrao, H. D., Heikal, A. A., Kasischke, K. A. & Webb, W. W. Conformational dependence of intracellular NADH on metabolic state revealed by associated fluorescence anisotropy. *J. Biol. Chem.* **280,** 25119–25126 (2005).